MODELLING OF MARFES AND OF EDGE RADIATION IN TOKAMAK PLASMAS INCLUDING KINETIC EFFECTS OF NON-MAXWELLIAN IMPURITIES

D. Reiser and M.Z. Tokar'

Institut für Plasmaphysik, Forschungszentrum Jülich GmbH, EURATOM Association, Trilateral Euregio Cluster, D-52425 Jülich, Germany

1. Introduction

The recently developed kinetic Monte-Carlo-code DORIS [1] has been proven to be a suitable tool to study the transport of impurities in tokamaks in the framework of a fully kinetic model. It combines in a consistent way results of a fluid model for the background plasma with drift kinetic and anomalous transport effects of the impurities, including ionization and recombination processes, Coulomb collisions with the background plasma and sputtering effects at the material boundaries. Distinct to other approaches [2] no hydrodynamic approximations are used in the description of impurities in order to account for the effects of collisions with an inhomogeneous background plasma and moreover the restriction on a cylindrical approximation is removed.
In this work results are presented for two species of impurities which are of great interest for the experiments at TEXTOR-94. Firstly the behaviour of carbon impurities after the onset of a MARFE (a radiative instability occuring at the high field side of TEXTOR-94, characterized by strongly localized high density and low temperature) is considered. Secondly, the transport of neon in the Radiative Improved Mode (RIM) [3] is analysed, using a selfconsistent modelling approach by coupling the Monte-Carlo-code DORIS with the fluid code RITM [4].

2. Drift Kinetic Model for Impurities

In the numerical model the following set of coupled drift kinetic equations is implemented:

$$\frac{\partial \bar{f}^Z}{\partial t} = -\frac{\partial}{\partial \boldsymbol{R}}\left(\dot{\boldsymbol{R}}\,\bar{f}^Z\right) - \frac{\partial}{\partial v_\parallel}\left(\dot{v_\parallel}\,\bar{f}^Z\right) - \frac{\partial}{\partial v_\perp}\left(\dot{v_\perp}\,\bar{f}^Z\right) + \bar{C}(\bar{f}^Z)$$

$$+\sum_{i,k}\frac{\partial^2}{\partial R_i \partial R_k}\left(\hat{r}_i\hat{r}_k\,D_\perp\,\bar{f}^Z\right) - S_I^Z\,\bar{f}^Z + S_I^{Z-1}\,\bar{f}^{Z-1} - S_R^Z\,\bar{f}^Z + S_R^{Z+1}\,\bar{f}^{Z+1} + Q_Z^+ - Q_Z^- \quad . \tag{1}$$

This governs the evolution of the transformed distribution functions $\bar{f}^Z = v_\perp f^Z$ of different charge states Z in time and in the 3D-2D phase space (3D in real and 2D in velocity space). The coefficients in the first three terms on the rhs are given by the equations of motion in the drift kinetic variables $\boldsymbol{R}$, $v_\parallel$ and $v_\perp$:

$$\begin{aligned}\dot{\boldsymbol{R}} &= v_\parallel\,\boldsymbol{b} + \frac{\boldsymbol{E}\times\boldsymbol{B}}{B^2} + \frac{1}{2}\,\frac{v_\perp^2}{\Omega}\,\frac{\boldsymbol{b}\times\boldsymbol{\nabla}B}{B} - \frac{v_\parallel^2}{\Omega}\,\boldsymbol{b}\times(\boldsymbol{b}\times(\boldsymbol{\nabla}\times\boldsymbol{b})) \\ \dot{v_\parallel} &= \frac{Ze}{m}\,\boldsymbol{E}\,\boldsymbol{b} + \frac{1}{2}\,v_\perp^2\,\boldsymbol{\nabla}\,\boldsymbol{b} \quad ; \quad \dot{v_\perp} = -\frac{1}{2}\,v_\parallel v_\perp\,\boldsymbol{\nabla}\,\boldsymbol{b} \quad ,\end{aligned} \tag{2}$$

with $\boldsymbol{b} = \boldsymbol{B}/B$ and $\Omega = ZeB/m$, $\boldsymbol{B}$ and $\boldsymbol{E}$ denote the electric and magnetic field, repspectively, m impurity mass and e elementary charge. $\bar{C}(\bar{f}^Z)$ is the drift kinetic Coulomb collision term

given by

$$\bar{C}(\bar{f}) = -\frac{\partial}{\partial v_\parallel}\left(K_\parallel \bar{f}\right) - \frac{\partial}{\partial v_\perp}\left(K_\perp \bar{f}\right) + \frac{1}{2}\frac{\partial^2}{\partial v_\parallel^2}\left(D_{\parallel\parallel} \bar{f}\right) + \frac{1}{2}\frac{\partial^2}{\partial v_\parallel \partial v_\perp}\left(D_{\parallel\perp} \bar{f}\right) + \frac{1}{2}\frac{\partial^2}{\partial v_\perp \partial v_\parallel}\left(D_{\perp\parallel} \bar{f}\right) + \frac{1}{2}\frac{\partial^2}{\partial v_\perp^2}\left(D_{\perp\perp} \bar{f}\right) \quad . \tag{3}$$

The drift and diffusion coefficients $K_\parallel$,. . .,$D_{\perp\perp}$ describe the interaction of the impurities with a slightly distorted maxwellian background [1]. The remaining terms in equation (1) describe sources and sinks due to ionization, recombination etc. and an anomalous diffusion in real space ($D_\perp$ is the diffusion coefficient, $\hat{\boldsymbol{r}}$ the radial unit vector).

3. Studies on carbon radiation in MARFEs

MARFEs are generally observed on the high field side of a tokamak, where the radial heat transport has a minimum. This can cause an instability effect due to the radiation of intrinsic impurities or due to strongly enhanced localized recycling of hydrogen. In our calculation we

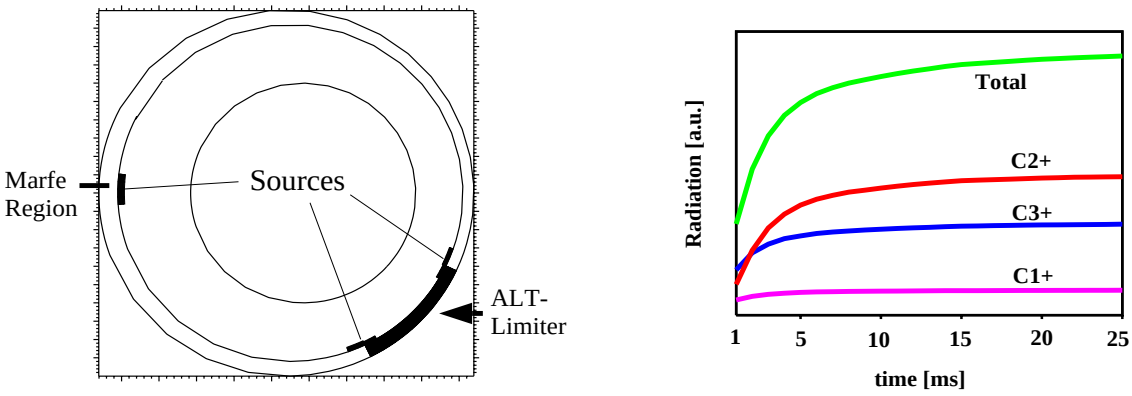

Fig. 1: Poloidal cross section of TEXTOR-94 and time evolution of carbon radiation.

study the case with localized recycling as the trigger for the MARFE and calculated the density and temperature profiles using a model suggested in [5], neglecting the influence of the intrinsic impurity carbon. Carbon serves as an indicator for a MARFE in experiments at TEXTOR-94, because its development is always accompanied by a rise of C^{2+}- and C^{3+}-radiation in the MARFE region. To clarify the origin of this enhanced radiation we have taken different sources of carbon into account and calculated the transport of carbon on background profiles after the onset of the MARFE. Fig. 1 shows a sketch of the poloidal cross section of TEXTOR-94 indicating the location of the carbon sources. Firstly a calculation was made taking into account only sources of carbon at the graphite ALT-II pump limiter due to physical sputtering by deuterium. The results demonstrated that this kind of source could not explain the radiation enhancement, because almost no carbon reached the MARFE region. In a second calculation we included a localized source at the wall, i.e. in the MARFE region, which led to a strong radiation in the MARFE, rising with a characteristic time of about 5 ms (Fig. 1). This characteristic time is by a factor of 2.5 smaller than in experimental observations [6]. We concluded that this

can be explained by an additional carbon source already existing before the MARFE onset. An additional simplified 1D calculation (along the field lines) assuming a homogeneous initial distribution of carbon in the MARFE region provided a characteristic rise time of about 10 ms closer to the experiment. To study those additional sources not included in the 2D calculation presented above a more detailed 2D modelling of the background plasma is necessary to get information about the origin of the carbon at the wall. A more fundamental result concerns the thermal forces acting on the impurities as a consequence of the steep temperature gradients at the MARFE borders. These play a dominant role in the transport of impurities along the field lines and depend strongly on the velocity distribution of the low ionized carbon impurities, i.e. their non-maxwellian character [1]. Fig. 2 shows the results of two calculations done with different assumptions for the thermal force.

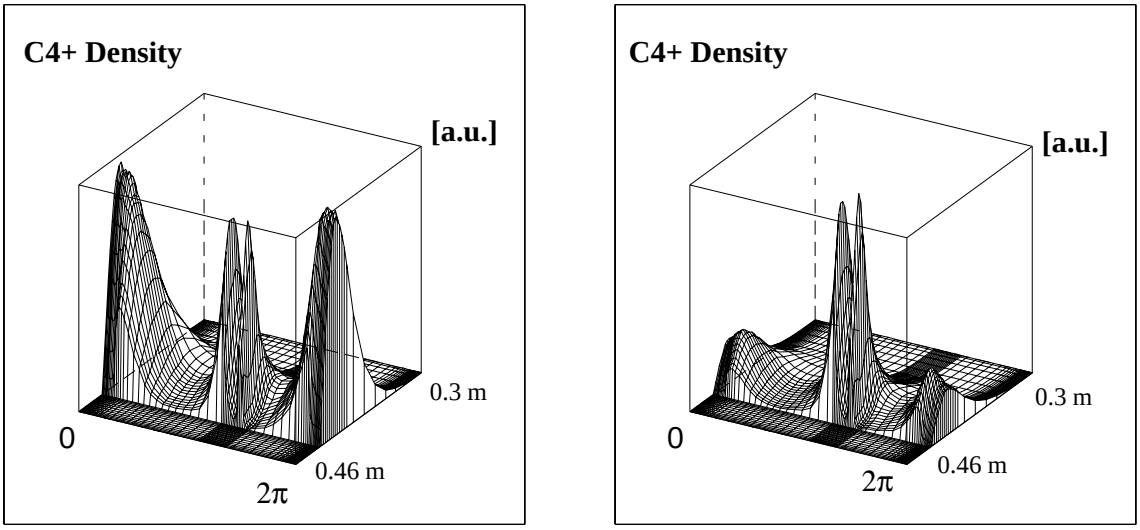

Fig. 2: C^{4+}-density distribution for fluid (left) and kinetic (right) description of the thermal forces.

In the first we assumed the thermal force to be 'fluid-like', i.e. we have taken into account the force acting on a maxwellian ensemble of impurities. In the second we have taken into account the correct 'kinetic' thermal force acting on a single impurity without the assumption of a maxwellian ensemble. Strong differences in the density distribution of the low ionized carbon ions occur (e.g. C^{4+} in Fig. 2). The fluid-like force overestimates the effect and leads to a much stronger localization of the carbon in the vicinity of the ALT-limiter (located at 0 or 2π, respectively), whereas the kinetic results exhibit a stronger localization in the MARFE region. This different behaviour indicates the non-maxwellian character of the low ionized carbon.

4. Studies on neon radiation in the plasma edge

Neon is a favorable candidate for the radiation cooling of the plasma edge; in addition, seeding of neon leads to an improvement of energy confinement as e.g. RI-mode in TEXTOR-94 [3]. A 2D modelling effort should clarify the influence of the source distribution of neon in the gas puff experiments. Fig. 3 shows the flux surface averaged 1D distribution of the higher charged neon species for different sources of the gas puffs in our calculation. We calculated the neon transport for three different localized sources in the

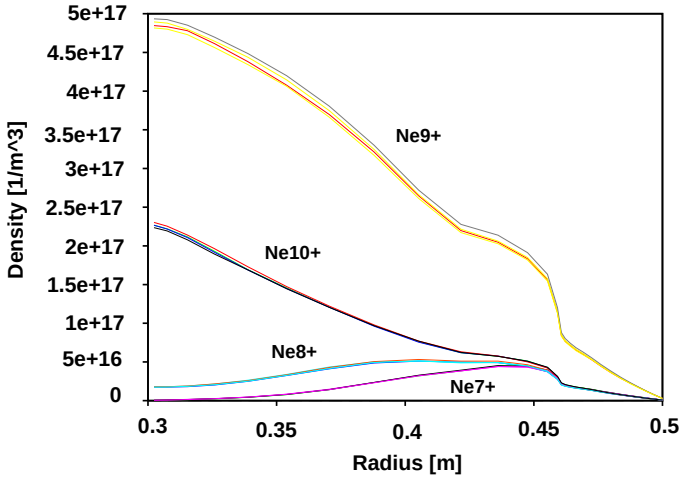

Fig. 3: Radial density distribution

SOL and also for an homogeneous source in the SOL. The results are almost identical demonstrating that the neon distribution is mainly determined by the radial transport of ions and by the recycling at the walls due to its low chemical reactivity. This allows to neglect the 2D details in the neon modelling and makes it a good candidate for 1D modelling efforts. Time dependent calculations done with a combination of the 1D-fluid code RITM and DORIS show a fairly good agreement with the experimentally observed tendencies of the formation of a radiating layer of neon accompanied by a cooling of the edge (see Fig. 4) and a rise in the electron density (not shown).

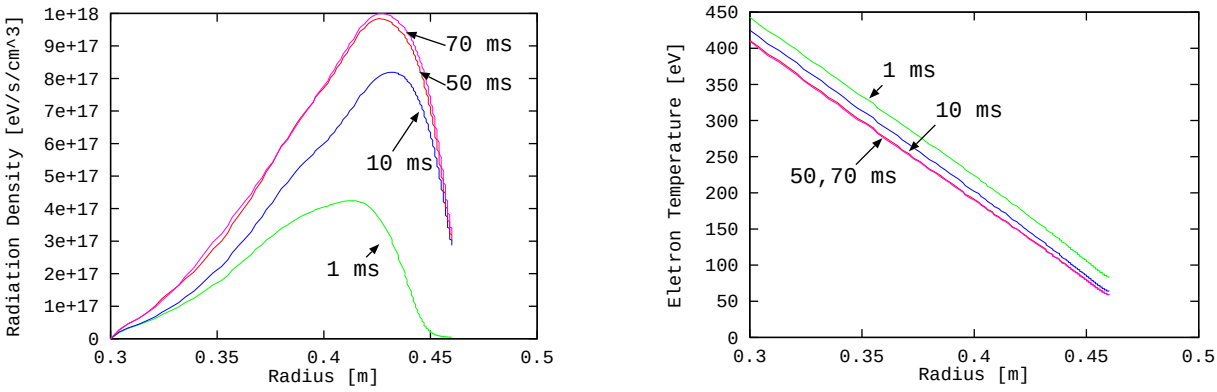

Fig. 4: Time evolution of Ne radiation density and electron temperature

References:

[1] Reiser, D., Reiter, D. and Tokar', M. Z.: "Improved Kinetic Test Particle Model for Impurity Transport in Tokamaks". Nuclear Fusion **38** (1998) 165

[2] Stangeby, P. C. and Elder, J. D.: J. Nucl. Mat. **196/198** (1992) 258

[3] Ongena, J.P.H.E.: "Overview of Plasma Performance with Edge Radiation Cooling in Limiter and Divertor Tokamaks". *This conference*

[4] Tokar', M. Z.: Plasma Phys. Contr. Fusion **36** (1994) 1819

[5] Tokar', M. Z. et al.:*Proceedings of the 12th PSI conference*, San Diego (1998)

[6] Samm, U. et al.: *Proceedings of the 12th PSI conference*, San Diego (1998)